

The influence of 180° ferroelectric domain wall width on the threshold field for wall motion

Samrat Choudhury,¹ Yulan Li,¹ Nozomi Odagawa,² Aravind Vasudevarao,¹ L. Tian,¹ Pavel Capek,³ Volkmar Dierolf,³ Anna N. Morozovska,⁴ Eugene A. Eliseev,⁵ Sergei Kalinin,⁶ Yasuo Cho,² Long-qing Chen,¹ and Venkatraman Gopalan^{1,a)}

¹Materials Science and Engineering, Pennsylvania State University, University Park, Pennsylvania 16802, USA

²Research Institute of Electrical Communication, Tohoku University, 2-1-1 Katahira Aoba-ku Sendai 980-8577, Japan

³Physics Department, Lehigh University, 16 Memorial Drive, Bethlehem, Pennsylvania 18015, USA

⁴V. Lashkarev Institute of Semiconductor Physics, National Academy of Science of Ukraine, 41 pr. Nauki, 03028 Kiev, Ukraine

⁵Institute for Problems of Materials Science, National Academy of Science of Ukraine, 3 Krjijanovskogo, 03142 Kiev, Ukraine

⁶Materials Science and Technology Division and Center for Nanophase Materials Sciences, Oak Ridge National Laboratory, Oak Ridge, Tennessee 37831, USA

(Received 11 August 2008; accepted 27 August 2008; published online 30 October 2008)

Unlike ideal 180° ferroelectric walls that are a unit cell wide (~ 0.5 nm), real walls in ferroelectrics have been reported to be many nanometers wide (1–10 nm). Using scanning nonlinear dielectric microscopy of lithium niobate (LiNbO₃) and lithium tantalate (LiTaO₃) ferroelectrics, we show that the wall width at surfaces can vary considerably and even reach ~ 100 nm in places where polar defects adjoin a wall. The consequence of such variable wall widths is investigated on the specific property of threshold field required for wall motion. Using microscopic phase-field modeling, we show that the threshold field for moving an antiparallel ferroelectric domain wall dramatically drops by two to three orders of magnitude if the wall was diffuse by only ~ 1 – 2 nm, which agrees with experimental wall widths and threshold fields for these materials. Modeling also shows that wall broadening due to its intersection with a surface will influence the threshold field for wall motion only for very thin films (1–10 nm) where the surface broadening influences the bulk wall width. Such pre-existing and slightly diffuse domain walls with low threshold fields for wall motion may offer a general mechanism to explain significantly lower experimental coercive fields for domain reversal in ferroelectrics as compared to the thermodynamic predictions. © 2008 American Institute of Physics. [DOI: 10.1063/1.3000459]

I. INTRODUCTION

Topological defects in materials play a critical role in understanding their real-world physical behavior. For example, dislocations explain the low deformation stresses required to overcome the otherwise large intrinsic Peierls potential barrier predicted for a perfect lattice.^{1,2} Additionally, the threshold stress to move a dislocation is inversely proportional to the spatial extent of the local stress field around a dislocation.³ Similarly, the coercive field to move a magnetic domain wall decreases exponentially as the wall width increases.⁴ Thus, one might expect similar trends in ferroelectrics, which contain two or more switchable states of built-in electrical polarization under the application of an electric field. In ferroelectrics, the inverse relationship between a ferroelectric wall width and threshold field is not intuitive besides being experimentally challenging to verify. This is because, unlike magnetic walls, a ferroelectric domain wall is theoretically predicted to possess an intrinsic width on a unit cell level (< 0.5 nm).⁵

Here we show that antiparallel domain walls in lithium niobate (LiNbO₃) and lithium tantalate (LiTaO₃) can become

diffuse on tens of nanometer scale in real ferroelectrics. We also show using phase-field modeling that even a broadening of the wall on 1–2 nm scale in the bulk can dramatically lower the domain wall threshold field by orders of magnitude, bringing them in agreement with experimental threshold fields. These two facts, taken together, imply that the motion of pre-existing and slightly diffuse ferroelectric domain walls can be a mechanism to explain low threshold fields for domain reversal in ferroelectrics.

This paper is organized as follows. In Sec. II, we discuss the experimental ferroelectric wall widths in literature as well as new scanning nonlinear dielectric microscopy (SNDM) results that show significant wall broadening in the 100 nm range at surfaces. In Sec. III, we present the microscopic phase-field modeling that explores the possible influence of wall broadening in the bulk and on the surfaces of ferroelectrics on the threshold coercive fields needed to move the wall. Finally, in Sec. IV, we discuss the conclusions of the study as regards correlation between the experimental wall widths and threshold fields in ferroelectrics.

II. EXTENDED FERROELECTRIC WALL WIDTH

Broadening of a domain or twin wall on nanometer scale due to extrinsic defects,^{6–8} charged walls,⁹ and surfaces^{10,11}

^{a)}Electronic addresses: vgopalan@psu.edu and vxg8@psu.edu.

has been observed. Direct imaging of strain,^{12,13} index contrast,¹⁴ and other optical properties^{15,16} at domain walls reveal property changes in length scales of 1–30 μm .¹⁷ The surface broadening also appears to be a sensitive function of the nature of the surfaces, including its electrostatic boundary condition, preparation, and defects.¹⁸ Recent work on carefully extracting the polarization profile across a ferroelectric wall using experiments and theory of piezoelectric force microscopy (PFM) reveals surprising statistical variation in wall widths on the surface, with widths of up to 100 nm as the tip radius approaches zero.¹⁹ However, zero tip radius is not possible to be experimentally achieved in a contact PFM imaging mode; hence direct imaging of such broadening is challenging with PFM. In comparison with the PFM technique, SNDM has a higher demonstrated spatial resolution, primarily arising from the localized region from where higher order dielectric permittivity tensors being probed arise.

Figure 1 shows SNDM images of a domain wall on the surface of thin single crystal slices of *z*-cut congruent lithium niobate [Figs. 1(a) and 1(b)] and lithium tantalate [Figs. 1(c) and 1(d)]. The basic principle is a phase-sensitive detection of the nonlinear capacitance of the sample.²⁰ An oscillating frequency ($\omega_p=6$ kHz) applied between the probe and the sample modulates the capacitance (ΔC_p) due to the linear and nonlinear dielectric response of the sample. This signal is detected by shifts in the resonance of an *LC* oscillator circuit that incorporates the tip. The capacitance change ΔC_p is thus measured at ω_p , $2\omega_p$, and $3\omega_p$ frequencies, which respectively correspond to the second, third, and fourth order dielectric constants of the sample. The signal of *n*th order dielectric constant is proportional to (*n*–1)th power of the alternating applied electric field at ω_p ; thus higher order signals have higher lateral resolution and sensitivity. Cho *et al.*²¹ have recently demonstrated imaging of the Si(111)7 \times 7 surface atomic structure using similar second and third order capacitance terms in SNDM showing <0.5 nm resolution of SNDM. From the line profiles of SNDM signal shown in Figs. 1(e) and 1(f), it is clear that the thinnest ferroelectric wall width in terms of dielectric contrast is ~ 20 nm. At places, this contrast can be even extended up to 50–100 nm as is particularly clear in Figs. 1(c) and 1(f), profile 5, where apparently a large polar dielectric defect touches the wall. Profile 3 in Figs. 1(b) and 1(e) shows that the second harmonic SNDM signal can reveal broadening that is not seen in the first order signal in Fig. 1(a). Similar studies in lithium tantalate,²² performed in cross-sectional *y*-cut geometry of the crystal reveals that the wall width decreases inside the crystal down to a width of ~ 2.5 –1 nm at a depth of ~ 50 –100 nm from the *z*-surface of the crystal. This demonstrates that the resolution of the system is <1 nm in such ferroelectrics. The results also clearly suggest that the local domain wall polarizability is different from the matrix domain, and that the domain wall width is influenced both by dielectric defects and by surfaces. This is also supported by the reported observation of a silent TO₉ Raman mode that appears only at the domain wall and involves Nb–O bond polarizability.²³

Thus, SNDM also reveals a wide spatial variation in wall

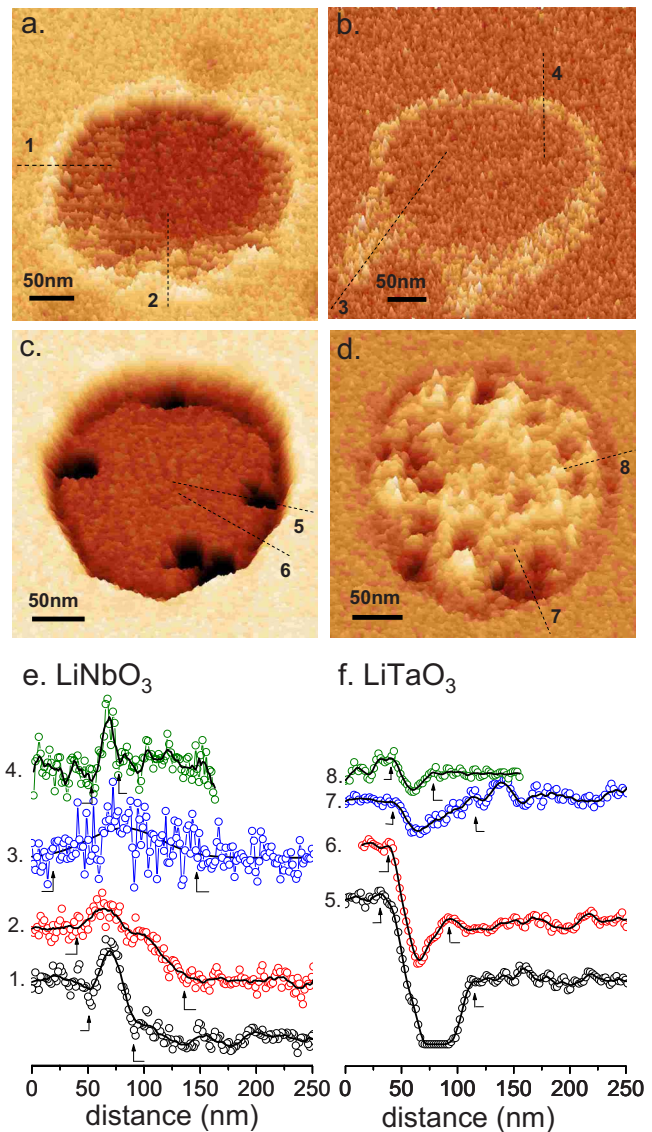


FIG. 1. (Color online) SNDM images of a circular domain in a 40 nm thick *z*-cut single crystal lithium niobate [(a) and (b)] and a 31 nm thick *z*-cut single crystal lithium tantalate [(c) and (d)] at first harmonic, $\omega_p=6$ kHz [(a) and (c)] and second harmonic, $2\omega_p=12$ kHz [(b) and (d)] modulation frequencies. Figures 1(d) and 1(e) show typical line profiles from these images as labeled, and pairs of arrows indicate the wall region. Images (a)–(d) are plotted in three-dimensional orthographic view with an $\sim 21^\circ$ rotation about the horizontal axes of the images. The length scales directly correspond to the horizontal axes of the images. The same domain region is imaged in (a) and (b), and similarly in (c) and (d).

width on the surfaces, ranging from 20 to 100 nm. A similar variability of a factor of 5 arising from bulk polar defects may also exist in the wall width in the bulk of the crystal, but it has not been systematically explored thus far. One could therefore expect a variation of ~ 1 –5 nm wall width in the bulk of the crystal. Next we explore the influence of such wall width and the influence of surfaces on the threshold fields for wall motion.

III. THRESHOLD FIELDS FOR WALL MOTION

A. Threshold field versus coercive field

We should first distinguish the ferroelectric coercive field and the threshold field for domain wall motion. The

coercive field is typically defined as the field values E_c corresponding to the crossings of the polarization hysteresis loops depicting P versus E . The coercive field corresponds to a field value where, on the average, equal areas of positive and negative domains exist in the probe region. The threshold field E_h for wall motion, on the other hand, corresponds to the field value at which a pre-existing domain wall begins to move after overcoming the intrinsic Peierls friction of the ferroelectric lattice. This field can be much lower than the coercive field E_c . The coercive field E_c depends not only on the field needed for nucleating a domain or moving a domain wall but also the field value needed for *long-range* motion of a wall by depinning through pinning sites in a ferroelectric. On the other hand, the threshold field E_h is just the field needed to begin to move a wall, which could even be a *local* pinned motion of bowing of the wall between two pinning sites. If the material already has pre-existing domain walls (which is in reality always the case), and if pinning is not strong (which is not always the case), then E_c can be similar to E_h . In this paper, we focus on E_h .

Bandyopadhyay and Ray²⁴ predicted the upper limit for E_h for domain walls of finite width, $2\omega_o$ as $E_h \leq a\alpha_{33}P_s/\omega_o$. For the uniaxial trigonal ($3m$) ferroelectric lithium niobate (LiNbO_3), the Landau coefficient $\alpha_{33} = 1/2\varepsilon_{33} \sim 2 \times 10^9 \text{ N m}^2/\text{C}^2$, where ε_{33} is the dielectric permittivity, the spontaneous polarization $P_s \sim 0.75 \text{ C/m}^2$, and the lattice parameter, $a = 0.515 \text{ nm}$, by which a 180° wall moves laterally. Thus, according to Bandyopadhyay and Ray,²⁴ $E_h \leq 30000 \text{ kV/cm}$ (LiNbO_3) and $\leq 12500 \text{ kV/cm}$ (LiTaO_3) for a unit cell sharp domain wall, $2\omega_o = a$. In contrast, the experimental coercive fields for LiNbO_3 are typically in the range from $E_c \sim 2 \text{ kV/cm}$ (stoichiometric composition) to 210 kV/cm (for congruent composition). The increase in the coercive field with deviation from the stoichiometric composition is known to be directly related to the increased pinning of domain walls. Even in nonstoichiometric (congruent) LiNbO_3 where $E_c = 210 \text{ kV/cm}$, the threshold field to bow a domain wall pinned between defect sites has been observed to be $E_h \leq 15 \text{ kV/cm}$, although it is only an upper limit.²⁵ If we exclude the influence of pinning by considering only the stoichiometric compositions of these materials, the domain walls are destabilized by electric fields as low as $\sim 0.5 \text{ kV/cm}$ in lithium tantalate and $\sim 2 \text{ kV/cm}$ in lithium niobate, which we believe are good estimates for the upper limits for threshold fields E_h for domain wall motion in these materials. It is thus important to distinguish the average coercive field E_c , which can be influenced by domain wall pinning events, and the threshold coercive field E_h to locally move a wall, which can be smaller than E_c and is the subject of this study. Next, we theoretically and numerically explore the relationship between E_h and wall width, $2\omega_o$, for LiNbO_3 and LiTaO_3 .

B. Analytical theory

Suzuki and Ishibashi²⁶ and later Sidorkin²⁷ have shown analytically for a one-dimensional (1D) system that the threshold field E_h to move a domain wall by overcoming the Peierls barrier of a 1D lattice decreases exponentially as a

function of increasing domain wall width. Recent works of Catalan *et al.*²⁸ and Shin *et al.*²⁹ have explored the role of internal structure of the domain wall itself on the domain reversal process. Following the outlines of the Ishibashi model^{26,30} (see Appendix A), we can derive a dependence of the threshold field E_h on the wall width $2\omega_o$ as follows:

$$E_{h,\text{Ishibashi}} = \alpha_{33}P_s \left(\frac{\omega_o}{a}\right)^3 \exp\left(-\frac{\pi^2\omega_o}{a}\right) e^4 \left(\frac{\pi}{2}\right)^{7/2}, \quad (1)$$

where all the terms are as defined in Sec. III A. One can clearly see an exponential drop in the threshold field for domain wall motion as a function of the wall width, ω_o . Next we present microscopic phase-field modeling of this dependence that includes the complete energy expression.

C. Microscopic phase-field modeling

The analytical theory of Suzuki and Ishibashi²⁶ uses a free energy expression described in Eq. (A1) in Appendix A that considers only the polarization energy describing the double potential well and a gradient energy term that incorporates the domain wall in the system. The elastic and electrostrictive terms were ignored, which we now consider in a numerical analysis. The complete analytical Ginzburg–Landau–Devonshire total free energy for the prototype paraelectric phase ($\bar{3}m$) of LiNbO_3 and LiTaO_3 in terms of order polarization vector P_i and strain tensor ε_{ij} is given by

$$F = \int \left[-\frac{\alpha_{ij}P_iP_j}{2} + \frac{\beta_{ijkl}P_iP_jP_kP_l}{4} + \frac{C_{ijkl}e_{ij}e_{kl}}{2} - \gamma_{ijkl}\varepsilon_{ij}P_kP_l + \frac{g_{ij}}{2} \left(\frac{\partial P_j}{\partial x_i}\right)^2 - \frac{P_iE_{i,dd}}{2} - P_iE_{i,\text{ext}} \right] dV, \quad (2)$$

where α_{ij} and β_{ijkl} are the first and second order impermittivity tensors and C_{ijkl} , γ_{ijkl} , and g_{ij} are the elasticity, electrostrictive, and gradient tensors, respectively. The numerical values for all these quantities in LiNbO_3 and LiTaO_3 are given in Ref. 31. Further, e_{ij} is strain, $E_{i,\text{ext}}$ is the external electric field, $E_{i,dd}$ the field due to dipole-dipole interactions, and V is the simulation volume. A single infinite domain wall with a polarization profile $P = P_s \tanh(x/\omega_o)$ is defined, where P_s is the spontaneous saturation polarization, x is the coordinate normal to the wall, and coordinate z is parallel to P_s . The wall is parallel to the crystallographic y -direction. A single 180° domain wall was placed in the simulation volume of $128a \times 2a \times 128a$ for a smaller gradient coefficient or $512a \times 2a \times 128a$ for a large gradient coefficient when the wall width $2\omega_o$ increased above $\sim 2 \text{ nm}$. Note that this is a quasi-two-dimensional (2D) simulation, picked to minimize the computational time, which even for three dimensions can be presently considerable. We verified using example simulations with a larger thickness than $2a$ that the final results we present are insensitive to this dimension.

Two cases were considered.

Case 1, bulk simulation. A single domain wall in an infinite ferroelectric medium with no surfaces. Since there are no surfaces, periodic boundary conditions were assumed in all directions x_i .

Case 2, thin crystal simulation. A single wall in a ferroelectric crystal of finite film thickness t in the polarization direction with top and bottom electrodes. The film thickness was taken as $t=na$ with $n<128$. Periodic boundary conditions were employed in x_1 and x_2 directions.

The spontaneous polarization, $\mathbf{P}=(P_1, P_2, P_3)$, is taken as the order parameter. The temporal evolution of the polarization pattern is calculated from solving the following time-dependent Ginzburg–Landau equations

$$\frac{\partial P_i(\mathbf{r}, t)}{\partial t} = -L \frac{\delta F}{\delta P_i(\mathbf{r}, t)} \quad (i = 1, 2, 3), \quad (3)$$

under the boundary condition of charge neutral surfaces specified as $\partial P_3 / \partial x_3 = 0$ at both $x_3 = 0$ and $x_3 = t$, the thickness of the ferroelectric film. [The coordinates (x_1, x_2, x_3) correspond to (x, y, z) .] Here L is the kinetic coefficient and F is the total free energy defined in Eq. (2), integrated over the volume of simulation. Note that without any applied stress, an internal stress field may be generated in a ferroelectric nanostructure by inhomogeneous spontaneous strains due to the inhomogeneous polarizations and the film surface boundary condition. The stresses must satisfy the mechanical equilibrium equation of $\sigma_{ij,j} = 0$ and stress-free top and bottom surface boundary conditions of $\sigma_{3j}|_{x_3=0} = \sigma_{3j}|_{x_3=t} = 0$. Periodic boundary conditions are assumed in the x_1 and x_2 coordinates.

Without any applied electric field or free charges, the electric field is induced only by the inhomogeneous spontaneous polarizations under the given boundary conditions. The self-electrostatic field is the negative gradient of the electrostatic potential, i.e., $E_i = -\phi_{,i}$. The electrostatic potential can be obtained by solving the electrostatic equilibrium equation,

$$\varepsilon_{11}(\phi_{,11} + \phi_{,22}) + \varepsilon_{33}\phi_{,33} = P_{1,1} + P_{2,2} + P_{3,3}. \quad (4)$$

Here, $\varepsilon_{11} = 54\varepsilon_0$ and $\varepsilon_{33} = 44\varepsilon_0$ for LiTaO₃ and $\varepsilon_{11} = 85\varepsilon_0$ and $\varepsilon_{33} = 30\varepsilon_0$ for LiNbO₃, respectively, and ε_0 is the vacuum permittivity. For simulating the domain wall switching, the boundary conditions of $\phi_3|_{x_3=0} = 0$ and $\phi_3|_{x_3=t} = \phi_0$ are imposed, where ϕ_0 is the applied external electric potential.

During the simulation, the gradient coefficient g_{13} was normalized to $g_0 = \alpha_{33}a^2$, the polarization was normalized to P_s and the grid spacing was chosen to be $\Delta x_1 = \Delta x_2 = \Delta x_3 = \Delta x = a$. The saturation polarizations $P_s = 0.75 \text{ C m}^{-2}$ for LiNbO₃ and $P_s = 0.5 \text{ C m}^{-2}$ for LiTaO₃ were assumed, and $a = 0.515 \text{ nm}$ was assumed. A single 180° domain wall was placed in the simulation volume. The threshold field was determined as the field E_h needed to move the wall by one unit cell distance a laterally. To include the lattice-pinning effect on domain wall motion, we adopt a microscopic version of the free energy model (1) defined on a lattice of perovskite unit cells. In this microscopic model, the Landau free energy becomes the local potential for the dipoles on each unit cell, and gradient energy terms describe the nearest-neighbor interactions. We note that there is no direct experimental measurement of the gradient coefficient g_{ij} of a material. In literature, one uses diffraction,³² electron microscopy,⁹ and scanning probe techniques¹⁹ to measure the width of interfaces such as twin walls and domain walls. The

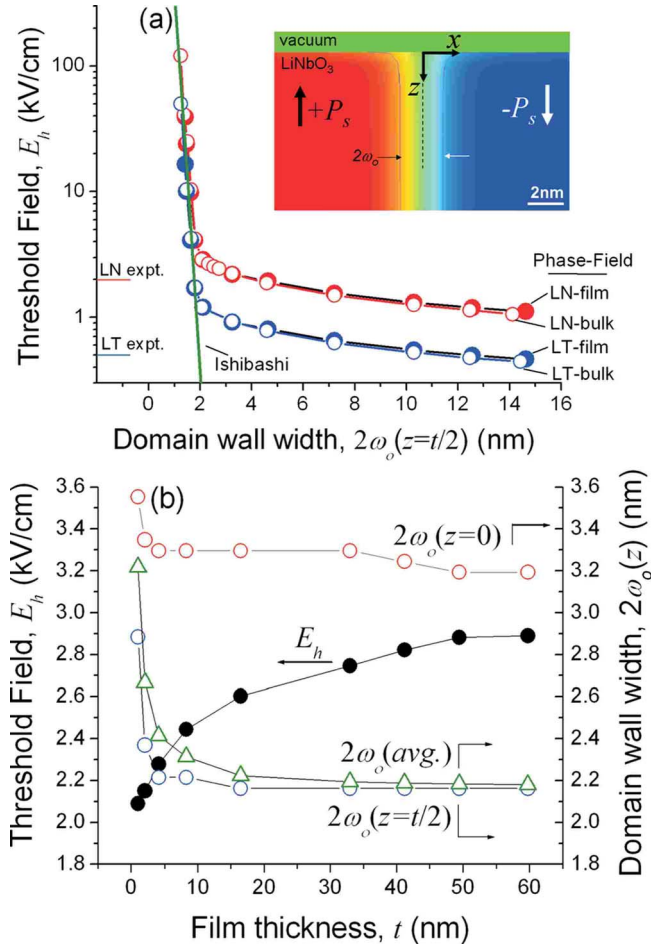


FIG. 2. (Color online) (a) Phase-field simulation of the threshold coercive field E_h for the motion of a single domain wall in LiNbO₃ (LN) and LiTaO₃ (LT) vs domain wall width $2\omega_o$. The film in phase-field simulation was $t = 96a$ thick, and the simulation size was $128a \times 2a \times 128a$ for $2\omega_o < 2 \text{ nm}$ and $512a \times 2a \times 128a$ for $2\omega_o > 2 \text{ nm}$, where $a = 0.515 \text{ nm}$. The phase-field simulation of the polarization profile at the junction between the wall and one of the surfaces of the film. The bulk phase-field simulation was infinite in all dimensions. Analytical theory based on Eq. (1) is also plotted for LiNbO₃. (b) The dependence of E_h on film thickness for a fixed $g_{13} = 4\alpha_{33}a^2$. Also the domain wall, $2\omega_o$ at $z=0$, $z=t/2$ and an average quantity, $2\int\omega_o(z)dz/t$ are plotted.

gradient coefficient, g_{ij} is typically determined from experimental wall width, as $\omega_o \sim \sqrt{2g_{13}/\alpha_{33}}$. Since we find the wall width ω_o to have experimental variability in this work, it is perfectly reasonable to assume that defect-wall interactions, such as in Fig. 1, can influence the gradient energy coefficient of the material. Thus we vary *only* the gradient coefficient g_{13} in the simulation, while keeping *all* other material properties the same.

D. Threshold field versus wall width

Figure 2(a) shows the threshold field E_h versus wall width $2\omega_o$ for the two numerical phase-field modeling cases, as well as the analytical theory. A striking observation is that even a small broadening of $2\omega_o \sim 2\text{--}3 \text{ nm}$ can dramatically lower coercive fields in these materials for both cases 1 and 2.

Note that while the wall width is uniform through the crystal for case 1, the wall broadens at the surface for case 2 as shown in the inset, where $t=96a$ was assumed. However, the E_h is in excellent agreement between cases 1 and 2, when the wall width $2\omega_o$ at $z=t/2$ is plotted for case 2 in Fig. 2(a). Thus an important conclusion is that for thick crystals, the bulk wall width determines the E_h , suggesting that the bulk of the wall exerts a drag on the surface triple junction under an external field. The results also show an excellent agreement between the Ishibashi model³⁰ and the phase-field modeling for small wall widths ($\omega_o < 2$ nm). For larger widths, phase-field modeling shows a second exponential dependence of the E_h versus ω_o that is different from the Ishibashi model. An analytical expression that approximates the phase-field modeling results is

$$E_h = A + B \exp\left(-\frac{\omega_o}{a\pi^2}\right) + E_{h,\text{Ishibashi}}, \quad (5)$$

where $A \sim 0.6$ kV/cm, $B \sim 1.798$ kV/cm for LiNbO₃. Although the elastic and electrostrictive energy terms are ignored in the Suzuki and Ishibashi model, but included in the phase-field modeling, their contribution is small and does not explain the difference between the two. There appears to be lattice friction components in the phase-field simulation that is not captured in the Ishibashi model. There is a frictional component [suggested by A in Eq. (5)] that is independent of the wall width and another component (described by the Ishibashi model) for small wall widths that leads to a strong dependence of the threshold field on the wall width. The intermediate exponential term [denoted by amplitude B in Eq. (5)] bridges these two wall width regimes. The physical origin of these additional lattice friction terms is presently unclear and may require atomistic modeling.

We next show that only in very thin crystals or films does the surface broadening of the wall influence the E_h . In such cases, the broadening of the wall at the two opposite surfaces interact and effectively broaden the bulk wall width itself at the center of the crystal. If $z \sim d$ is approximately the crystal depth to which the wall broadening occurs due to the presence of a surface, then $t \sim 2d$ would be the crystal thickness at which the surfaces would begin to influence the threshold field for domain wall motion. This is seen more clearly in Fig. 2(b) by plotting the correlation between E_h and the integrated average wall width over the crystal thickness, given by $\omega_{\text{eff}} = 2\int \omega_o(z)dz/t$, for a fixed gradient coefficient g_{13} . Clearly the threshold field decreases as the bulk wall width increases due to a decrease in the crystal thickness. Note that while conventional nucleation models³³ predict an *increase* in the coercive field E_c with thinner films, the threshold field E_h is predicted to remain unchanged for thicknesses much greater than the surface wall broadening depth d and *decreases* only when t approaches $2d$. Since in the LiNbO₃ and LiTaO₃ sample studied here, the coercive field E_c *does not* change over a thickness range from 900 nm (thinnest sample studied here) to 0.5 mm (thickest studied), we expect that the nucleation model of Landauer³³ and Janovec³⁴ are not the dominant mechanisms for explaining the observed coercive field E_c for wall motion. Instead, the growth of pre-existing microdomains in the crystals requir-

ing a threshold field E_h to grow and a depinning field E_c to overcome pinning sites is more relevant. This would also predict that the threshold coercive field will decrease for thinner single crystal LiNbO₃ and LiTaO₃ of $t \sim 1-10$ nm due to surface effects.

IV. DISCUSSION

From Fig. 2, in LiNbO₃, the threshold electric field decreases drastically, a change of two orders of magnitude (from 787 to 1.95 kV/cm), with an increase in domain wall width from $2\omega_o \sim 0.76$ nm to $2\omega_o \sim 2.1$ nm. For larger domain wall widths, another order of magnitude decrease is observed, reaching a value of ~ 0.3 kV/cm for a wall width of $2\omega_o \sim 103$ nm. Similar results are seen for LiTaO₃, but with lower coercive fields. To put these results in context, the estimated threshold field for bulk LiNbO₃ crystals to date is ~ 2 kV/cm and for LiTaO₃ is ~ 0.55 kV/cm. This would correspond to a bulk wall width of ~ 2 nm for LiNbO₃ and ~ 2.7 nm from Fig. 2. These are entirely reasonable values based on the experimental results on wall widths known for these materials as discussed in Sec. II.

Interestingly, the bulk width of a given wall determines the threshold field for motion of the entire wall. For a homogeneous crystal of thickness $z=t$, the wall thickness at $t/2$ appears to determine the threshold field for the motion of the wall. Figure 1 shows that even 100 nm wall widths are locally possible near defects and at surfaces; however, these defects will influence the overall threshold field for wall motion only if they influence the bulk wall width. This bulk wall width broadening, however, does not have to be large. Even a broadening from 0.5 to 2 nm will dramatically lower the threshold field for motion by a few orders of magnitude.

Finally, we address a more subtle question: is the dramatic drop in the threshold field E_h versus the wall width $2\omega_o$ in Fig. 2 due to an increase in the wall width, or due to a corresponding increase in the wall energy σ ? After all, by varying the gradient coefficient, g_{13} , as done here, the domain wall energy $\sigma \propto \sqrt{g_{13}\Delta f}$ also changes, where $\Delta f \sim \alpha_{33}^2/4\beta_{3333}$ is the Landau energy barrier. For the simulation of a real material such as LiNbO₃ or LiTaO₃, these two effects, namely, the influence of wall width versus the wall energy on the threshold field is difficult to separate. To avoid confusion from the discussion that follows, we reiterate that the only variable in Fig. 2 is the gradient coefficient, g_{13} . No other material parameter was varied in Fig. 2, and thus those results should be considered valid for the materials studied here. However, we can perform numerical tests on a ‘‘hypothetical material’’ as described in Appendix B, which confirms the central role of wall width instead of wall energy in the decrease of threshold coercive field in ferroelectrics.

V. CONCLUSIONS

This work explores the correlation between domain wall width and the threshold field for wall motion. SNDM images show that wall widths in ferroelectric lithium niobate and lithium tantalate can be quite extended (~ 100 nm), particularly when polar defects adjoin a domain wall. The role of such broadening, whether due to defects or surfaces is ex-

plored on the threshold field required to move the wall. Using microscopic phase-field modeling and analytical theory, we find that the threshold field drops dramatically by two to three orders of magnitude with an increase in the bulk wall width to even ~ 2 nm, which is consistent with the wall widths and threshold fields reported for these materials in literature. Interestingly, we predict that wall broadening at surfaces will influence the threshold field only when the crystal thickness is on the order of 1–10 nm, where the surfaces influence the bulk wall properties. In general, the bulk wall region with the narrowest width will dominate the threshold field for the motion of the entire wall. Pre-existing and slightly diffuse domain walls with low threshold fields for wall motion may provide one general mechanism to explain significantly lower experimental coercive fields for domain reversal relative to their thermodynamic predictions in all ferroelectrics.

ACKNOWLEDGMENTS

We would like to gratefully acknowledge NSF Grant Nos. DMR-0507146, DMR-0512165, DMR-0820404, DMR-0602986, ARO Grant No. W911NF-04-1-0323 and DOE Grant No. DE-FG02-07ER46417. Research was also sponsored in part by the Division of Materials Sciences and Engineering, Office of Basic Energy Sciences, U.S. Department of Energy, under Contract No. DE-AC05-00OR22725 and CNMS2008-289 with Oak Ridge National Laboratory.

APPENDIX A: ANALYTICAL DERIVATION OF THE THRESHOLD FIELD

The following development follows the Suzuki and Ishibashi model.²⁶ Free energy density for a one component ferroelectric, ignoring tensor notation, is given by

$$f(x) = -\frac{\alpha}{2}P(x)^2 + \frac{\beta}{4}P(x)^4 + \frac{g}{2}\left[\frac{dP(x)}{dx}\right]^2. \quad (\text{A1})$$

The equation of state is

$$-\alpha P(x) + \beta P(x)^3 - g\frac{d^2P(x)}{dx^2} = 0. \quad (\text{A2})$$

The solution of Eq. (A2), corresponding to an isolated domain wall, is

$$P(x) = P_S \tanh\left(\frac{x}{\omega_o}\right), \quad (\text{A3})$$

where $P_S = \sqrt{\alpha/\beta}$ is spontaneous polarization of a homogeneous system and $\omega_o = \sqrt{2g/\alpha}$ is a measure of the half-width of the wall [distance where the polarization reaches a value of $0.76P_S \approx \tanh(1)P_S$ from the center of the wall]. Introducing the designation $r(x) = P(x)/P_S$ we can rewrite Eq. (A1) as

$$\begin{aligned} f(x) &= -\frac{\alpha^2}{4\beta} + \frac{\alpha^2}{4\beta}[1 - r(x)^2]^2 + \frac{g}{2}\left(\frac{\alpha}{\beta}\right)\left[\frac{dr(x)}{dx}\right]^2 \\ &\equiv \left\{ \frac{K^2}{2}[(1 - r(x)^2)^2 - 1] + \frac{1}{2}\left[\frac{dr(x)}{dx}\right]^2 \right\} \left(\frac{\alpha g}{\beta}\right) \\ &\equiv \left\{ \frac{1}{2\omega_o^2} \left[\left(1 - \tanh\left(\frac{x}{\omega_o}\right)\right)^2 - 1 \right] \right. \\ &\quad \left. + \frac{1}{2}\left[\frac{d}{dx}\tanh\left(\frac{x}{\omega_o}\right)\right]^2 \right\} \left(\frac{\alpha g}{\beta}\right). \end{aligned} \quad (\text{A4})$$

The density of free energy excess localized at the wall is given by

$$f(x) + \frac{\alpha^2}{4\beta} \equiv \left(\frac{\alpha g}{\beta}\right) \frac{1}{\omega_o^2 \left[\cosh\left(\frac{x}{\omega_o}\right) \right]^4}. \quad (\text{A5})$$

Surface energy of the wall is

$$\int_0^\infty \left(f(x) + \frac{\alpha^2}{4\beta} \right) dx = \frac{3\alpha g}{4\beta\omega_o} \equiv \frac{3\alpha^2}{4\beta} \sqrt{\frac{g}{2\alpha}}.$$

Using the expression (A5) and results of Ishibashi,³⁰ it is easy to rewrite the activation energy between a stable (state I) and unstable (state II) domain wall positions as

$$\Delta F = F_{II} - F_I = a \sum_n \left[f(na) + \frac{\alpha^2}{4\beta} \right] - \int_{-\infty}^\infty \left[f(x) + \frac{\alpha^2}{4\beta} \right] dx.$$

where n is an integer that discretizes the lattice in units of lattice parameter, a . This can be further simplified as

$$\Delta F \approx \frac{\alpha^2}{\beta} \sqrt{\frac{2g}{\alpha}} \left(\frac{\sqrt{2g}}{a\sqrt{\alpha}} \right)^3 \exp\left(-\frac{\pi^2\sqrt{2g}}{a\sqrt{\alpha}}\right) e^4 \left(\frac{\pi}{2}\right)^{7/2}. \quad (\text{A6})$$

Ishibashi model stops with the derivation of ΔF , a key result. We can now obtain the threshold field for domain wall motion as

$$E_{h,\text{Ishibashi}} \sim \frac{\Delta F}{P_S\omega_o} = \alpha P_S \left(\frac{\omega_o}{a}\right)^3 \exp\left(-\frac{\pi^2\omega_o}{a}\right) e^4 \left(\frac{\pi}{2}\right)^{7/2}, \quad (\text{A7})$$

which completes the derivation of Eq. (1). The thermodynamic coercive field, on the other hand, is given by

$$E_c = 2\alpha\sqrt{\alpha/(27\beta)}. \quad (\text{A8})$$

APPENDIX B: THE INFLUENCE OF DOMAIN WALL WIDTH VERSUS WALL ENERGY ON THE THRESHOLD FIELD

By varying the gradient coefficient, g_{13} , the domain wall energy $\sigma \sim \sqrt{g_{13}\Delta f}$ also changes, where $\Delta f \sim \alpha_{33}^2/4\beta_{3333}$ is the Landau energy barrier. In order to determine if the change in threshold coercive field E_h is due to a change in the wall width $2\omega_o$ or the wall energy σ , we repeated the simulation in Fig. 2(a) by performing the following two numerical tests.

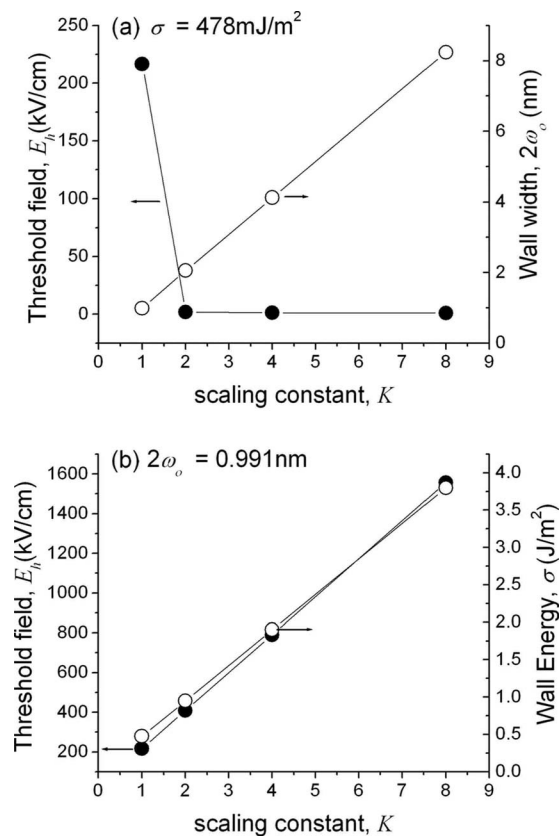


FIG. 3. Numerical test to test the influence of wall width $2\omega_o$ versus wall energy, σ . (a) Scaling g_{13} by a constant K , while scaling α_{33} , and β_{33} , by $1/K$, and (b) g_{13} , α_{33} , and β_{33} are all scaled by K .

- (a) Fix σ and P_s , while varying wall width $2\omega_o$: by arbitrarily scaling g_{13} by a constant K ($K > 1$), while scaling α_{33} , and β_{33} , by $1/K$, we linearly scale the wall width, $\omega_o \sim P_s \sqrt{g_{13}/\Delta f}$ by a factor K , while keeping the wall energy σ and the saturation polarization $P_s = \sqrt{\alpha_{33}/\beta_{33}}$ constant. The results are shown in Fig. 3(a), where clearly a dramatic drop in E_h is seen with scaling of the wall width in a bulk crystal.
- (b) Fix $2\omega_o$ and P_s , while varying wall energy σ : if g_{13} , α_{33} , and β_{33} are all scaled by K , the wall width σ and polarization P_s remain the same, while the wall energy scales linearly by K . Figure 3(b) shows that this leads to a linear increase in the threshold coercive field for a single domain wall in a bulk crystal.

Although scaling α_{33} and β_{33} in the above numerical tests changes the material itself (and hence these results do

not correspond to LiNbO₃ or LiTaO₃ any more, but instead to a hypothetical material), these tests do confirm the central role of wall width instead of wall energy in the dramatic decrease of threshold coercive field in Fig. 2(a).

- ¹R. E. Reed-Hill, *Physical Metallurgy Principles* (PWS-Kent, Boston, 1991).
- ²F. R. N. Nabarro, *Philos. Mag. A* **75**, 703 (1997).
- ³W. Benoit, M. Bujard, and G. Gremaud, *Phys. Status Solidi A* **104**, 427 (1987).
- ⁴J. I. Arnaudas, A. Del Moral, and J. S. Abell, *J. Magn. Magn. Mater.* **61**, 370 (1986).
- ⁵J. Padilla, W. Zhong, and D. Vanderbilt, *Phys. Rev. B* **53**, R5969 (1996).
- ⁶W. T. Lee, E. K. H. H. Salje, and U. Bismayer, *Phys. Rev. B* **72**, 104116 (2005).
- ⁷M. Calleja, M. T. Dove, and E. K. H. Salje, *J. Phys.: Condens. Matter* **15**, 2301 (2003).
- ⁸D. Shilo, G. Ravichandran, and K. Bhattacharya, *Nat. Mater.* **3**, 453 (2004).
- ⁹C-L. Jia, S-B. Mi, K. Urban, I. Vrejoiu, M. Alexe, D. Hesse, *Nature Mater.* **7**, 57 (2008).
- ¹⁰W. T. Lee, E. K. H. H. Salje, and U. Bismayer, *J. Phys.: Condens. Matter* **14**, 7901 (2002).
- ¹¹J. Novak and E. K. H. Salje, *J. Phys.: Condens. Matter* **10**, L359 (1998).
- ¹²T. Jach, S. Kim, V. Gopalan, S. Durbin, and D. Bright, *Phys. Rev. B* **69**, 064113 (2004).
- ¹³S. Kim, V. Gopalan, and B. Steiner, *Appl. Phys. Lett.* **77**, 2051 (2000).
- ¹⁴S. Kim and V. Gopalan, *Mater. Sci. Eng., B* **120**, 91 (2005).
- ¹⁵V. Dierolf and C. Sandmann, *J. Lumin.* **102–103**, 201 (2003).
- ¹⁶V. Dierolf and C. Sandmann, *J. Lumin.* **125**, 67 (2007).
- ¹⁷V. Gopalan, V. Dierolf, and D. A. Scrymgeour, *Annu. Rev. Mater. Res.* **37**, 449 (2007).
- ¹⁸E. A. Eliseev, A. N. Morozovska, Y. L. Li, L. Q. Chen, V. Gopalan, and S. V. Kalinin, e-print arXiv:0802.2559.
- ¹⁹L. Tian, A. Vasudevarao, A. N. Morozovska, E. A. Eliseev, S. Kalinin, and V. Gopalan, *J. Appl. Phys.* **104**, 074110 (2008); also, see e-print arXiv:0802.2900v1.
- ²⁰Y. Cho, A. Kirihara, and T. Saeki, *Rev. Sci. Instrum.* **67**, 2297 (1996).
- ²¹R. Hirose, K. Ohara, and Y. Cho, *Nanotechnology* **18**, 084014 (2007); also Y. Cho and R. Hirose, *Phys. Rev. Lett.* **99**, 186101 (2007).
- ²²Y. Daimon and Y. Cho, *Appl. Phys. Lett.* **90**, 192906 (2007).
- ²³V. Dierolf and C. Sandmann, *Appl. Phys. B: Lasers Opt.* **78**, 363 (2004).
- ²⁴A. K. Bandyopadhyay and P. C. Ray, *J. Appl. Phys.* **95**, 226 (2004).
- ²⁵T. J. Yang, V. Gopalan, P. J. Swart, and U. Mohideen, *Phys. Rev. Lett.* **82**, 4106 (1999).
- ²⁶I. Suzuki and Y. Ishibashi, *Ferroelectrics*, **64**, 181 (1985).
- ²⁷A. S. Sidorkin, *Ferroelectrics* **150**, 313 (1993).
- ²⁸G. Catalan, J. F. Scott, A. Schilling, and J. M. Gregg, *J. Phys.: Condens. Matter* **19**, 022201 (2007).
- ²⁹Y.-H. Shin, I. Grinberg, I.-W. Chen, and A. M. Rappe, *Nat. Mater.* **449**, 881 (2007).
- ³⁰Y. Ishibashi, *J. Phys. Soc. Jpn.* **46**, 1254 (1979).
- ³¹D. A. Scrymgeour, V. Gopalan, A. Itagi, A. Saxena, and P. J. Swart, *Phys. Rev. B* **71**, 184110 (2005).
- ³²K. R. Locherer, J. Chrosch, and E. K. H. Salje, *Phase Transitions* **67**, 51 (1998).
- ³³R. Landauer, *J. Appl. Phys.* **28**, 227 (1957).
- ³⁴V. Janovec, *Czech. J. Phys., Sect. A* **8**, 3 (1958).